Dynamic Light-Scattering Studies of the Fractal Aggregation of Poly(methacrylic acid) and Poly(ethylene glycol)

David J. Hemker and Curtis W. Frank*

Department of Chemical Engineering, Stanford University, Stanford, California 94305-5025

Received July 3, 1989; Revised Manuscript Received March 21, 1990

ABSTRACT: The complexation and subsequent aggregation of poly(methacrylic acid) (PMAA) with poly(ethylene glycol) (PEG) were investigated with photon correlation spectroscopy (PCS). The influence on aggregation of hydrophobic pyrene probes covalently attached to the PEG chain ends, denoted PEG*, was also studied. The effectiveness of PCS in determining average particle radius, $\langle R \rangle$, and particle radii distributions in aggregating polymer systems is demonstrated. The effect of pH on $\langle R \rangle$ and aggregation rate is examined. A critical pH of 1.9 was found, below which the system aggregates more rapidly into larger clusters. Under the proper solution conditions, the time dependence of the particle distributions can be monitored. We found a power law growth of $\langle R \rangle$ with time for both PMAA-PEG and PMAA-PEG*. This type of growth behavior is consistent with a cluster-cluster type model of aggregation. The tagged system showed much more rapid aggregation and larger $\langle R \rangle$. An aggregation model assuming Smoluchowski kinetics and diffusion-limited, cluster-cluster aggregation was developed. An excellent fit between the model and data was obtained, with the aggregates showing fractal scaling with a fractal dimension of 1.7.

Introduction

Association reactions between polymers in aqueous media have been extensively studied due to their important role in colloidal suspensions, micellar systems, and associative thickeners. In our earlier work in this area, we examined polymer complexation reactions driven by hydrogen bonding and hydrophobic association.[1-5] Specifically, we examined molecular level details of PEG before and after complexation with PMAA or PAA. By using a fluorescent pyrene probe covalently bound to the ends of the PEG chains, we obtained detailed information about complex conformation. Several system parameters, such as component polymer molar ratio, degree of polyacid neutralization, extent of hydrophobicity of the system, and pH, were varied in order to study the effects on local chain conformation. This resulted in several conclusions, which are summarized in the following.

One important finding was the significant enhancement in complexation resulting from the presence of the hydrophobic α-methyl group in PMAA.[5] It was shown that there was significant hydrophobically driven clustering between the PMAA and the pyrene groups attached to the PEG chain ends. This association went above and beyond the expected association due to hydrogen bonds between PEG and PMAA. This finding means that the pyrene probes used in the fluorescent measurements are not as benign as initially thought, since they perturb the intrinsic complexation between PEG and PMAA. One of the goals of the present study is to further investigate the effects of the pyrene probes on solutions of PMAA-PEG and, if possible, to quantify these perturbations.

The primary motivation for the present work, however, came from the observation that, as the pH of a PMAA-PEG solution was lowered, the solution became more turbid. Tsuchida and co-workers[6,7] have identified this phenomenon as arising from the aggregation of the polymer complexes. Using total intensity light scattering and turbidity measurements, they showed that as time increased more light was scattered from the PMAA-PEG solutions, implying the formation of larger and larger aggregates. They also demonstrated that aggregation was enhanced by increasing the polymer concentration, increasing the temperature, or decreasing the solution pH. Moreover, a critical pH was found, above which the complexes did not aggregate over a time scale of tens of minutes. Below this critical pH, aggregation was greatly enhanced. They briefly outlined a particle-cluster aggregation scheme but gave no evidence supporting this model.

Our objective in this paper is to extend our previous spectroscopic measurements of complexation to the next larger size scale by examining the aggregation of the polyacid-PEG complexes. The primary tool we use is photon correlation spectroscopy (PCS), which allows us to accurately determine an average aggregate size, the distribution of sizes, and the kinetics of aggregation. We will use the results of Tsuchida et al.[7] as a starting point and as an aid in determining the proper solution conditions (e.g., temperature, pH, concentration) for our study. Finally, we present a very simple model for the size distribution of the aggregates and the time dependence of this distribution.

Experimental Section

Materials. The PMAA and PEG used in this study were the same as described previously.[1] Pyrene-end-labeled poly(ethylene glycol) (PEG*) was synthesized by direct esterification between poly(ethylene glycol) (PEG) and 1-pyrenebutyric acid. The polydispersity of the PEG* was checked by gel permeation chromatography and was found to be the same as the PEG starting material (<1.10). The PEG* was determined to be fully labeled at both ends with ±5% accuracy via UV absorption measurements.

Solution Preparation. Aqueous solutions of 4×10^{-3} M PMAA, PEG, and PEG*, based on repeat unit concentration, were made by using distilled deionized water. The water was first passed through a 0.22-μm filter to remove any dust particles before dissolving the polymer. The solutions were kept in a water bath at 303 K so minimal thermal equilibration time was necessary when the samples were transferred to the index-matching bath of the PCS apparatus that was also at 303 K. Before a PCS measurement was taken, equal volumes of PMAA and PEG or PEG* were added to a 12-mm round cuvette resulting in equimolar 2×10^{-3} M solutions. The pH of a solution was controlled by adding microliters of filtered, concentrated HCl with a micropipet.

Photon Correlation Spectroscopy (PCS). In the PCS apparatus, the incident radiation is supplied by a Lexel 2-W argon ion laser operating at 514.5 nm. The sample holder is centered in a thermostated index-matching bath that is mounted on the pivot point of an optical rail holding the detector. The scattering

0024-9297/90/2223-4404$02.50/0

angle is selected by pivoting the rail around the index-matching bath. The scattered light is collected by an iris diaphragm and then focused by a 100 mm focal length lens onto a 100-μm pinhole. The light that passes through the pinhole is then focused by the detector optics onto a photomultiplier tube (PMT). The output of the PMT is sent to an amplifier–discriminator, and the resultant signal is sent to a Brookhaven BI2020 136-channel, 4-bit correlator. The last eight channels are time multiplexed so as to give readings for long correlation times. This allows the data in these channels to be used as a measured base line. The data from the correlator are then transferred to an IBM-AT compatible microcomputer for further analysis.

All measurements were done by using 12-mm cylindrical cuvettes at an angle of 90°. Sample times were chosen such that the data at long correlation times decayed to less than 20–50% of the data in the first channel. Another criterion used for selecting the sample time was to maximize the number of channels over which the decay occurred. This allows for the highest possible resolution. The total number of samples for each measurement was kept constant at 10^7. This resulted in average measurement times of ~15–60 s per solution. A measurement was discarded if the total number of correlator overflows was greater than 0.1% of the total number of counts in the first channel.

The analysis software calculates an expected value for the decay data at infinite time. For each measurement, this calculated base line was compared with the measured base line taken from the average of the eight long time-delay channels. If the two values differed by more than 0.2%, the data from that run were discarded. This procedure helped minimize the effects of dust in the scattering solution, since dust would result in the measured base line being significantly higher than the calculated base line. For the purposes of data analysis, the calculated base line was generally used in all data manipulations.[32]

PCS Data Analysis. The autocorrelator receives a value from the PMT proportional to the light-scattering intensity $I(t)$ and computes the second-order temporal correlation function[33-35]

$$G^{(2)}(\tau) = \langle I(0)I(\tau)\rangle \tag{1}$$

This can be normalized to give

$$g^{(2)}(\tau) = \frac{G^{(2)}(\tau)}{\langle I\rangle^2} \tag{2}$$

where $\langle I\rangle^2$ is the measured or calculated base line described above and is given by

$$\lim_{\tau_L\to\infty} G^{(2)}(\tau_L) = \langle I\rangle^2 \tag{3}$$

The first-order correlation function can be related to the second-order correlation function by

$$g^{(2)}(\tau) = 1 + C|g^{(1)}(\tau)|^2 \tag{4}$$

where C is an adjustable parameter dependent on factors such as instrument geometry and clipping levels but is independent of τ. The general first-order correlation function written in terms of hydrodynamic radius, R, is[35]

$$g^{(1)}(\tau) = \int_0^\infty F(R)\exp\left\{-\left[\left(\frac{q^2kT}{6\pi\eta}\right)R^{-1}\tau\right]\right\} dR \tag{5}$$

where

$$q = \frac{4\pi n}{\lambda}\sin\frac{\theta}{2} \tag{6}$$

and k = Boltzmann constant, T = absolute temperature, η = viscosity of solvent, n = refractive index of the solution, λ = wavelength of incident light, θ = scattering angle, and $F(R)$ = amount of light scattered by particles of size R. Equation 5 assumes the scattering particles are undergoing Stokes–Einstein diffusion.

The primary goal of the PCS data analysis is to obtain a reasonable estimate of $F(R)$ given a series of measured $G^{(2)}(\tau)$. To perform the inversion of eq 5 and obtain $F(R)$, the program CONTIN[36,37] was used. The strength of CONTIN lies in that it requires no initial information as to the number of relaxation modes present in the data.[38] The ability of CONTIN to accurately determine the relaxation times of bimodal systems has been demonstrated,[35] along with its ability to correctly determine $F(R)$ for polydisperse monomodal experimental systems with known particle size distributions.[39] CONTIN performs an inverse Laplace transform that directly outputs the smoothest nonnegative solution for $F(R)$ that is consistent with the signal to noise ratio for the data.[31] The output is given in terms of hydrodynamic radii observed and their relative scattering intensities. No dust correction term was deemed necessary, since no change in the output was observed when the term was included in the analysis. Data were initially fit over a large radii range. Higher resolution was obtained in subsequent runs by using a smaller, optimized radii range in order to spread the data out over the calculation grid. A data analysis was considered statistically meaningful if the reported standard deviation was less than 10^{-3}.

Results

The initial system chosen for examination with PCS consisted of a solution of PMAA and unlabeled PEG in water at 25 °C. The concentrations of both PMAA and PEG were 2×10^{-3} M based on repeat units. The pH of the equimolar mixture was adjusted to 2.75 with concentrated HCl. On the basis of the results of Tsuchida,[7] these conditions should result in measurable changes in aggregate size on a time scale of tens of minutes. The conditions, with the exception of the lowered pH, are identical with those of our previous work.[5] Note that the only difference between the system used by Tsuchida and our system is the polymer molecular weights. Tsuchida[7] used PMAA and PEG molecular weights of 40 000 and 6000, respectively, while ours were 9500 and 9200.

The fraction of light scattered by particles of a given radius in the solution described above, immediately after mixing, was determined by CONTIN. The particles range in size from ~20 to ~126 nm. In order to compare this result with other aggregation work we need to determine some "average radius", $\langle R\rangle$, of the distribution. If the normalized intensity distribution is called $F(R)$, then the moments of that distribution, M_j, can be calculated by

$$M_j = \int_0^\infty R^j F(R)\, dR \tag{7}$$

where R is the hydrodynamic radius of a particle. Following Flamberg and Pecora,[8] we have decided to define an average radius as

$$\langle R\rangle = M_0/M_{-1} \tag{8}$$

On the basis of this definition, the solution giving rise to the scattered light intensity distribution for pH 2.75 has an average radius of ~48 nm. This radius did not significantly change over the course of 100 min.

The possibility exists that the reason aggregation did not occur on the time scale observed by Tsuchida is because the pH was not low enough. Even though the pH chosen (2.75) was below the critical pH for Tsuchida's system, the difference in PMAA molecular weights may cause a shift in the critical pH since cooperation between adjacent hydrogen bonding sites is so important in these complexing systems.[9] Thus, the lower the molecular weight, the less likely that aggregation will occur under the same solution conditions. Therefore, we expect that a lower pH would be necessary to achieve the same rate of aggregation in a lower molecular weight system (i.e., the lower the pH, the higher the fraction of protonated carboxylic acid sites necessary to form hydrogen bonds). In order to test this hypothesis, we varied the pH of our PMAA–PEG solution with HCl and then measured the pH, the initial aggregate size, and the aggregation rate.

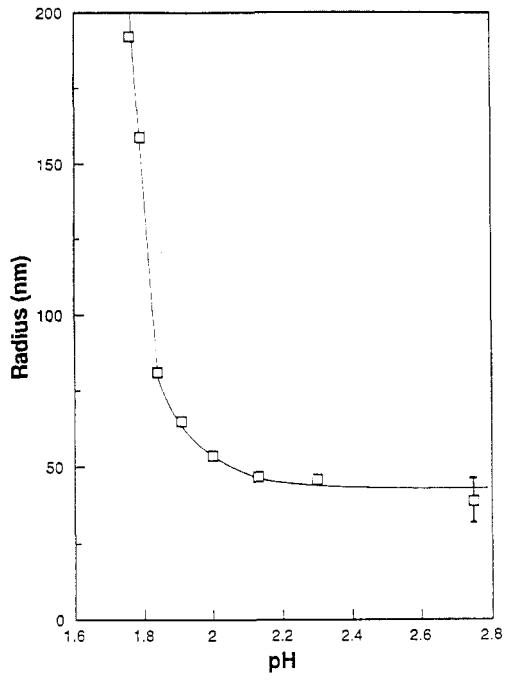

Figure 1. Average aggregate radius, $\langle R \rangle$, as a function of pH for PMAA–PEG immediately after mixing.

Figure 1 shows the initial average aggregate radius as a function of pH. This figure exhibits the same general behavior as the total scattered light intensity vs pH curve of Tsuchida, which showed a critical pH of 3. In the case of Figure 1, the critical pH has been shifted to a lower value of about 1.9 because of the lower molecular weight of our PMAA. Since the average radius of the solution with pH 2.75 did not change over a period of hours, it can be assumed that 48 nm is probably close to the equilibrium value for those conditions. Likewise, the kinetics of this system must be such that equilibrium is reached in less than 1 min, the approximate time it took to mix the solution and take the measurement.

There are many studies that show that complexation occurs rapidly, on the order of milliseconds.[7] However, depending on the reaction conditions, successive aggregation may or may not occur.[10] In order to investigate this aggregation process further, we attempted to find a set of conditions for which the kinetics would allow us to monitor the aggregation with PCS. This was accomplished by lowering the pH to the critical value of 1.9 found in Figure 1. Using these conditions, a definite time dependence of the average radius with time was observed. This increase in size with time is plotted in Figure 2 and is mathematically described by a power law relationship

$$\langle R \rangle = R' t^b \tag{9}$$

where t is time and R' and b are constants.

The data of Figure 2 were fit to eq 9 by using a least-squares criterion to obtain constants R' and b. This fit is shown as a straight line in Figure 2. The constant R' was calculated to be 68 nm, and b was found to be 0.11. A value for b greater than 1 indicates an ever accelerating reaction (the rate of increase in size increases with time). A value less than 1 indicates that the rate of size increase decreases with time. Since a single measurement requires approximately 1 min, the value of 68 nm for R' indicates that, on the PCS experimental time scale, the initial complexes were effectively this size. This parameter is not, however, related to aggregate size at real times approaching zero. In physical terms, we know that at $t = 0$ the system consists of individual polymer chains with radii on the order of tens of angstroms. Thus, R' should be thought of as a measure of aggregate size at an arbitrary time.

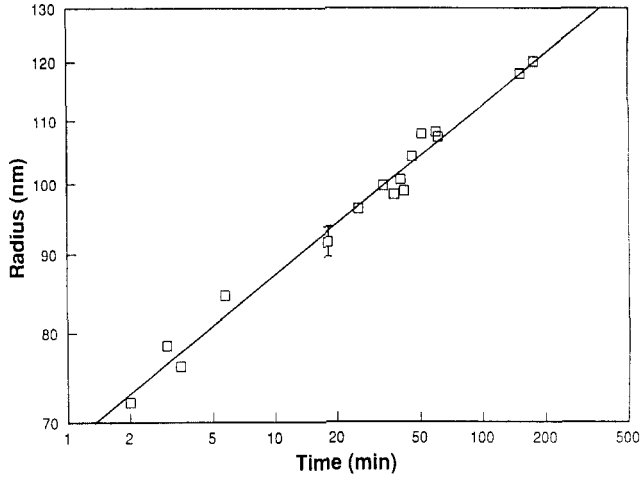

Figure 2. Rate of growth of the PMAA–PEG aggregate radius. Solution pH = 1.9. Straight line is a least-squares power law fit.

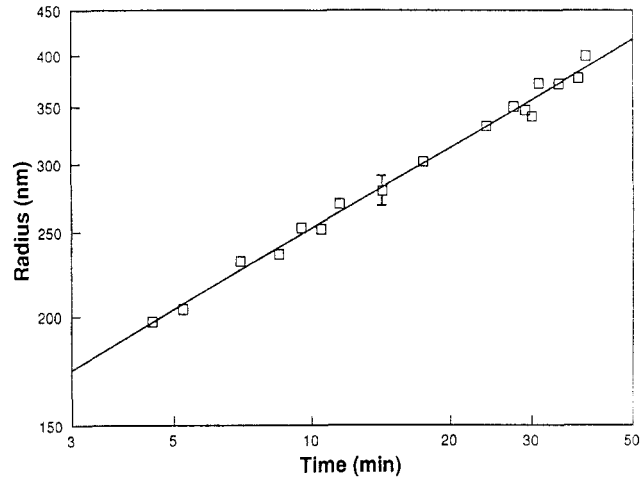

Figure 3. Rate of growth of the PMAA–PEG* aggregate radius. Solution pH = 3. Straight line is a least-squares power law fit.

In summary, a power law relationship accurately describes the time dependence of the average radius of this system over a restricted time range. Unfortunately, the asymptotic behavior at long and short times cannot necessarily be predicted with this model. The constants can, however, be used to compare rate data for different systems.

Since the preceding data have demonstrated the usefulness of PCS in the determination of aggregation size distributions and aggregation rates, we can now employ the technique to investigate differences between PMAA–PEG systems in which the PEG is tagged with pyrene, denoted as PEG*, and systems in which the PEG is untagged. Initially, an identical solution used to obtain Figure 2 was made with the exception of using labeled PEG instead of unlabeled PEG. However, when the first PCS measurement was made on the solution, approximately 1 min after mixing, the solution had already aggregated so rapidly that the average radius had reached ~1000 nm. In order to slow the aggregation process, a new solution with a pH of 3 was prepared.

The kinetic data for this solution are shown in Figure 3. As with the unlabeled system, the data follow a power law relationship with the constants $R' = 123$ nm and $b = 0.31$. The aggregation rate for the PMAA–PEG* system is much faster than in the system with unlabeled PEG. This observation manifests itself in the larger power law

exponent, b, for the PMAA–PEG*. The larger R' value indicates that, on the time scale PCS can monitor, the aggregate size at early times appears to be 123 nm compared to 68 nm for PMAA–PEG. Keep in mind that the measurements on the unlabeled system were done at pH 3 while those for the unlabeled data were taken with pH 1.9. If the reaction conditions were identical, the differences between the two aggregation rates would be even more pronounced. These results are the first quantitative proof that the pyrene probes greatly enhance the aggregation of these polymers.

Discussion

In the preceding section, we demonstrated the experimental feasibility of using PCS to monitor the distribution of particle sizes and the time evolution of that distribution in a solution of aggregating PMAA and PEG. We also showed a dramatic enhancement in aggregation rate when pyrene-end-labeled PEG is used. Additionally, the sensitivity of aggregate size to pH seen by Tscuchida[7] was reconfirmed.

In this section we propose a model that is capable of describing the aggregation process. Expressions for the distribution of particle radii and the time evolution of the distribution will be derived. We will then attempt to fit our data to the model and in the process determine the scaling of cluster sizes, limiting aggregation regimes, and mechanism of aggregation. We note that the molecular details of the "fundamental particles" implied by our simple model are not known. Our objective is to provide a semiquantitative treatment of the formation of larger structures that may be examined by PCS. Separate spectroscopic measurements[1-5] have been directed at the molecular level complexation.

In considering the basic problem of aggregation, there are two questions that must be answered. The first concerns the limiting step in the aggregation. The general process of aggregation involves two particles diffusing toward each other. When they are some characteristic distance apart, there is a certain probability that the interaction forces between the two particles will be such that the particles stick together (e.g., via a hydrogen bond). If the sticking probability is high in comparison to the diffusion rate of the particles, the process is known as diffusion-limited aggregation (DLA). If, on the other hand, the diffusion rate is high in comparison to the sticking reaction rate, the process is known as reaction-limited aggregation (RLA). In order to simplify the analytical models, generally either DLA or RLA is chosen as the dominant mechanism.

The second question that must be answered concerns the relative mobility of aggregates. Again, as above, two limiting cases exist. In the first, only the individual subparticles that make up all larger aggregates are allowed to diffuse. This model was first investigated in a computer simulation by Witten and Sander.[11] Aggregates grow via the addition of individual subparticles. This process is known as particle–cluster aggregation. This is analogous to the growth of a polymer chain via a free-radical polymerization.[12] The second limiting case allows both individual particles and all larger aggregates to diffuse freely. In this model, aggregates grow by the combination of two aggregates of any size. This process is known as cluster–cluster aggregation. A condensation reaction is the analogous model in polymerization terms. Schematic diagrams describing these two aggregation processes are shown in Figure 4.

As a starting point for the development of our model, we will assume our aggregation system is described by the

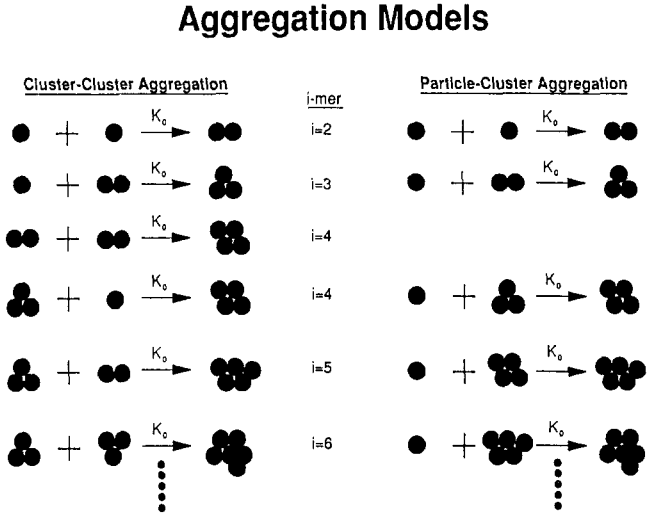

Figure 4. Schematic diagram illustrating mechanisms for aggregate growth in cluster–cluster and particle–cluster aggregation models.

diffusion-limited aggregation model and that cluster–cluster aggregation is the dominant mode for aggregate growth. The cluster–cluster model was chosen, since in experimental studies done on three-dimensional aggregation,[13-16] generally using gold colloids, this model was found to be valid. The choice of DLA over RLA was dictated by the dynamic behavior observed in Figures 2 and 3. Weitz et al.[17] found that, for a system of gold particles aggregating in the RLA regime, the particle radius grew exponentially with time. When the reaction conditions were changed so the growth was in the DLA regime, the average particle radius scaled with time via a power law relationship as did our data. These scaling behaviors are also predicted from a theoretical analysis of the two aggregation regimes.[29]

Our use of the cluster–cluster and DLA assumptions implies that aggregates are noninteracting until they stick together irreversibly on contact. The effects on aggregation of long-range interactions, such as dipole or screened Coulomb, have been investigated by Hurd.[18] We will assume they are negligible and will discuss their possible presence in our system after more fully developing our model. We will first derive a theoretical expression for the light-scattering intensity distribution as a function of radius. This will allow us to directly fit our CONTIN distributions and then test the agreement. However, as was mentioned above, this process is actually a fit of an estimated distribution. Therefore, the results must be checked for sensitivity to the actual fitting methods used in each step.

The time dependence of aggregate mass, assuming cluster–cluster aggregation, for a solution initially consisting of N_0 particles of radius R_0 can be described by the generalized Smoluchowski equations.[19,20] These can be written as

$$\frac{dN_i}{dt} = \frac{1}{2}\sum_{j=1}^{i-1} K_{j,i-j} N_j N_{i-j} - \sum_{j=1}^{\infty} K_{ij} N_i N_j \qquad (10)$$

where N_i is the number of aggregates formed from i particles (i-mer) and K_{ij} reflects the rate of aggregation of an i-mer with a j-mer. The first term on the right-hand side is the rate of formation of aggregates due to the aggregation of a j-mer and an $(i-j)$-mer. The second term reflects the rate of loss of i-mers due to their aggregation to form larger clusters. The form of the Smoluchowski diffusion kernel, K, in eq 10 is determined by either the

DLA or RLA assumptions. Also, it is straightforward to rewrite eq 10 in terms of a particle–cluster model. This is essentially done by fixing one of the interacting clusters, and its appropriate index in eq 10, to be a single particle.[20]

For DLA the diffusion kernel is equal to the sum of the capture radii for the two clusters times the sum of their diffusion coefficients[29]

$$K_{ij} = (R_i + R_j)(D_i + D_j) \tag{11}$$

If we assume that the capture radius scales with the cluster radius and that the clusters undergo Stokes–Einstein diffusion

$$K_{ij} = c \tag{12}$$

where c is a constant. This simplification can be made since $D \sim 1/R$, resulting in the radial dependence canceling in eq 11. This result signifies that the aggregation rate should be independent of cluster size.

Using the constant kernel assumption, eq 10 can be integrated to give the time dependence of an aggregation number distribution for cluster–cluster, diffusion-limited aggregation

$$\frac{N_i}{N_0} = \frac{A^{i-1}}{(1 + A)^{i+1}} \tag{13}$$

where $A = k_s N_0 t$. The constant k_s is the rate constant for the aggregation of any two clusters.

The next step is to write eq 13 in terms of aggregate radius, R_i, rather than number of subparticles. The most obvious procedure for calculating the radius of an i-mer would be to assume spherical aggregates of constant density, as in the following.

$$V_i = iV_0 \tag{14}$$

$$\frac{4}{3}\pi R_i^3 = i\frac{4}{3}\pi R_0^3 \tag{15}$$

$$i = \left(\frac{R_i}{R_0}\right)^3 \tag{16}$$

Equation 16 can be inserted into eq 13 to give an expression for the number distribution of particles in terms of the radius. This number distribution cannot, however, be directly compared with the light-scattering intensity distribution calculated by CONTIN.

In order to relate the two distributions, we follow the method of Flamberg and Pecora.[8] The expression relating intensity distribution to number distribution is

$$F(R) = B\alpha^2(R)\, f(R)\, S(R) \tag{17}$$

where $F(R)$ is the intensity distribution as calculated by CONTIN, B is a normalization constant, $\alpha(R)$ is the polarizability of a cluster of size R, $f(R)$ is the number distribution function, with $f(R)\,dR$ being the number of particles with radius R between R and $R + dR$, and $S(R)$ is the form factor.[21-23] In our case, $f(R)$ is simply the combination of eqs 13 and 16. α for spheres is given by CR^3, where C is a constant, and[24]

$$S(R) = [3/(qR)^3] \sin qR - qR \cos qR \tag{18}$$

where q is the scattering vector for the light-scattering measurement. In our measurements q is a constant, since all data were taken at a scattering angle of 90°.

The above derivation assumes that the aggregates obey the Rayleigh–Debye condition

$$(4\pi/\lambda)R[(n/n_0) - 1] < 1 \tag{19}$$

where λ = wavelength of scattered light, n = refractive index of particles, and n_0 = refractive index of medium. For our experimental conditions eq 19 is valid for all particles of radius less than ~750 nm. Thus, this condition is met for all distributions measured, except for the very high-end tail of the PMAA–PEG* system at aggregation times greater than about 35 min.

After appropriate substitutions, the normalized eq 15 becomes

$$F(R) = R^6\left(\frac{3}{(qR)^3} \sin qR - qR \cos qR\right)\frac{A^{(R/R_0)^3}}{(1 + A)^{(R/R_0)^3}} \tag{20}$$

Recall that R_0 is the radius of the initial particles present. Although the identity of the initial particles is somewhat ambiguous, it could be a single Gaussian coil, an intermolecular complex, or a highly compact cluster of collapsed chains. If we assume the initial particle is an individual polymer chain, we may take the root-mean-square end-to-end distance for our PEG chains of ~3 nm[25] as an estimate for R_0 in eq 20. The accuracy of this assumption will be checked later.

Before eq 20 can be fit to the light-scattering data, one more transformation is necessary. Due to the nature of the PCS experiments, the scattered light intensity distributions are biased toward larger particles. This results in a loss of sensitivity of small aggregates that are low in concentration. Therefore, before fitting we scale the radius in eq 20 by subtracting the minimum resolvable radius, R_{min}, from R. It should be emphasized that R_{min} is not an adjustable parameter; it is obtained directly from each CONTIN distribution.

Equation 20 was then fit to normalized CONTIN distributions by using a modified Levenberg–Marquardt–Simplex[26] method with the constant A as the only adjustable parameter. This fitting procedure was attempted for all of the distributions that gave the average radii reported in Figures 2 and 3. However, no value of A was found that would satisfy the least-squares criterion for any distribution. Therefore, we must refine the model.

A more general scaling is provided by

$$i = (R/R_0)^D \tag{21}$$

where D is the scaling dimensionality of the system. By allowing D to vary in the fitting procedure, a best fit estimate of the system dimensionality can be obtained. For this type of scaling, the polarizability becomes

$$\alpha(R) = C'R^D \tag{22}$$

where C' is a constant related to the average polarizability of an initial particle. Also, Martin and Schaefer[27] give the structure factor as

$$S(qR) = \frac{1}{(qR)^D} \tag{23}$$

where q is defined as before. This expression is valid for $qR \gg 1$. In our system qR ranges from ~1 to ~4.

Substituting eqs 13 and 21–23 into eq 17 yields

$$F(R) = R^D\left[\frac{A^{(R/R_0)^D}}{(1 + A)^{(R/R_0)^D}}\right] \tag{24}$$

for the normalized intensity distribution. When eq 24 was fit to the CONTIN output, convergence was obtained. This least-squares fitting process was repeated for each of the distributions for which the average radii are reported in Figures 2 and 3. An average dimensionality of 1.7 ± 0.25 was found for the aggregate distributions. This exponent was found in both the PMAA–PEG and PMAA–PEG*

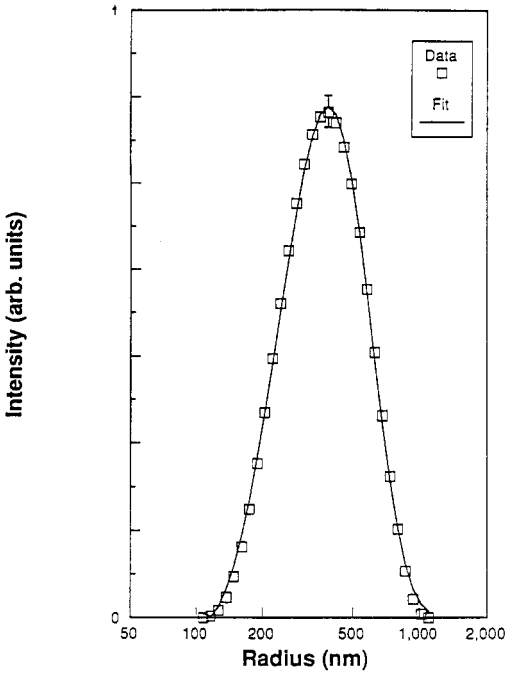

Figure 5. Aggregate size distribution for PMAA–PEG* at a pH = 3, 38 min after mixing. The line is the fit of the aggregation model to the CONTIN data. The calculated fractal dimension of this particular aggregate distribution is 1.69.

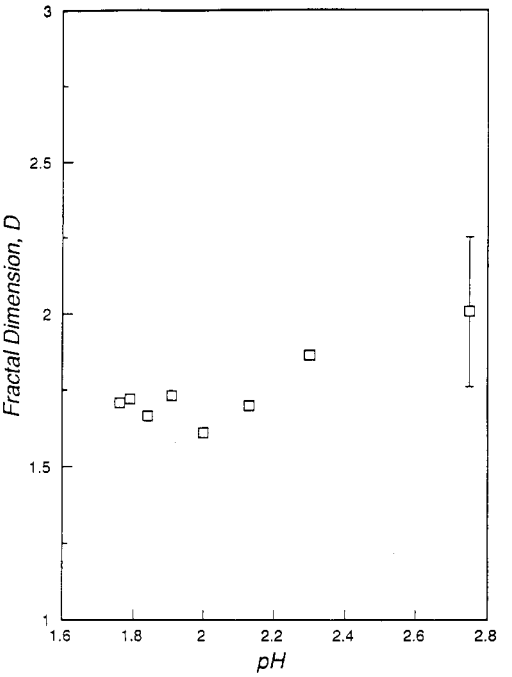

Figure 6. Variation of calculated fractal dimension with pH for PMAA–PEG immediately after mixing.

systems and was constant in time. Figure 5 shows a typical CONTIN distribution and the resulting fit of eq 24. The agreement between data and model is extremely good.

The uncertainty in D arises from many sources. The largest source of error is probably due to the fact that the data used to fit eq 20 are themselves a best fit of the actual measured scattering autocorrelation function. Although CONTIN represents the state-of-the-art method for obtaining intensity distributions, the calculated distributions are by no means exact. In fact, due to the nature of the inverse Laplace transform, the CONTIN calculated distribution is not necessarily unique. CONTIN reports several "solution" distributions, each characterized by a calculated probability to reject, α.[30] The closer α is to $^1/_2$, the "better" the solution as based on CONTIN's convergence criteria.[31] The sensitivity of D with respect to α was checked by fitting several less than optimal CONTIN solutions to eq 24. In each case the same fractal dimension, within the ±0.25 uncertainty, was found. This stability is helped by the fact that calculated CONTIN distributions are fairly stable for unimodal distributions of particles.[30]

The nonintegral exponent implies a system with dilational symmetry; i.e., the aggregates can be described as having "fractal" dimensionality.[28] Several computer simulations[13-15] have shown that cluster–cluster aggregation in the DLA regime should produce a dimensionality of 1.8. The microscopy experiments on diffusion-limited colloidal gold aggregates done by Weitz et al.[29] produced a fractal scaling of 1.7. Likewise, neutron and light scattering done on the same particles gave rise to a fractal exponent of 1.8. However, under reaction-limited aggregation conditions, Weitz et al.[17] found a fractal dimension of 2.0. The close agreement between these studies and our data supports our finding that the PMAA–PEG aggregates are fractal in nature and grow via DLA and cluster–cluster aggregation.

Our exponent of 1.7 also implies that there are negligible long-range interactions between clusters. A simulation done by Hurd[18] found that systems with screened coulombic interaction resulted in fractal dimensions of less than 1.7.

Using the same procedure as described above, eq 22 was fit to the distributions that gave rise to Figure 1, in order to determine the effect of pH on D. These data are presented in Figure 6. Note that there appears to be a slight increase in D from about 1.7 to 2 as the pH is raised. However, due to the large uncertainty in the data, the trend may not be real. If the increase is indeed real, this may be evidence that at higher pH reaction-limited aggregation and/or particle–cluster aggregation mechanisms are dominant.

Another parameter obtained from the fit of eq 24 was the constant A, from which, the reaction rate constant, k_s, can be calculated as described in eq 13. For PMAA–PEG aggregation, k_s is 0.5×10^{-14} min^{-1}, and for PMAA–PEG* aggregation, it is 1.7×10^{-14} min^{-1}. The uncertainty of these values is about ±70%. Note that the value of k_s has been normalized by the initial number of chains present and is therefore expressed on a per chain basis. The large scatter in the fitted values of A for each data set is reflected in the large uncertainty of each k_s. It is best to view these numbers as order of magnitude estimates rather than exact values. The most useful information from these calculations is that the rate constant for PMAA–PEG* aggregation is higher than that for PMAA–PEG. This is another piece of evidence demonstrating the enhancement in aggregation due to the hydrophobic clustering of the pyrene-end-labeled PEG chains.

If R_0 is considered a variable in eq 24, then the fitting procedure will give a best fit estimate of the parameter. When this was done, R_0 was calculated to be ~1.5 nm for the PMAA–PEG data and ~2.5 nm for the PMAA–PEG* data. Both numbers show reasonable agreement with the root-mean-square end-to-end distance of 3 nm used in the fitting procedure. Additionally, when R_0 was treated as a variable, the fit to the data still produced a D of 1.7. This indicates that D is somewhat insensitive to changes in R_0. These results also suggest that the initial particles in the tagged system are larger than those in the untagged system. Their molecular identity remains to be determined.

As an additional check of the validity of the DLA assumption, an attempt was made to fit the data to a

reaction-limited aggregation model. For RLA, it is assumed that the aggregation reaction rate is sufficiently slow that the two clusters can sample all possible mutual configurations before an aggregation reaction can occur. The probability of bonding is then proportional to the ratio of the number of bonding configurations (e.g., configurations when the clusters are touching) to the total number of possible configurations. The Smoluchowski kernel for this scenario is proportional to this bonding probability, which has been shown[29] to be proportional to the cluster mass

$$K_{ij} = i + j \tag{25}$$

Substituting eq 25 into eq 10 and integrating yields

$$\frac{N_i}{N_0} = \frac{(1 - B)e^{-iB}(iB)^{i-1}}{i!} \tag{26}$$

where B is related to the time dependence of the first moment of the distribution.[29]

Equation 26 was substituted into eq 17 and the fitting procedure was repeated. However, no solution was found that was able to describe the distribution data. Also, the particle–cluster solution of eq 10, using a constant kernel, likewise could not be fit to the data. These results indicate that our aggregation system may be characterized by cluster–cluster, diffusion-limited aggregation.

Summary

There are several important findings of this work. We have demonstrated the usefulness of PCS in determining average particle size and particle distributions in aggregating polymer systems. Under the proper solution conditions, the time dependence of the particle distributions can be monitored. We found a power law growth of $\langle R \rangle$ with time for both PMAA–PEG and PMAA–PEG*. The tagged system showed much more rapid aggregation, presumably due to the additional aggregation force from the hydrophobic attraction of the pyrene tags. An aggregation model assuming Smoluchowski kinetics and diffusion-limited, cluster–cluster aggregation was developed. An excellent fit between the model and data was obtained, with the aggregates showing fractal scaling with a fractal dimension of 1.7.

Acknowledgment. We thank Professors Alice Gast and Robert Pecora for their helpful discussions and useful suggestions. This work was supported by the Polymers Program of the National Science Foundation under Grant DMR 84-07847.

References and Notes

(1) Oyama, H. T.; Tang, W. T.; Frank, C. W. *Macromolecules* **1987**, *20*, 474.
(2) Oyama, H. T.; Tang, W. T.; Frank, C. W. *Macromolecules* **1987**, *20*, 1839.
(3) Frank, C. W.; Oyama, H. T.; Hemker, D. J. *Frontiers of Macromolecular Science*; Saegusa, T., Higashimura, T., Abe, A., Eds., 1989, pp 337–342.
(4) Hemker, D. J.; Garza, V.; Oyama, H. T.; Frank, C. W. *Complexation of Poly(acrylic acid) and Poly(methacrylic acid) with Pyrene End-Labeled Poly(ethylene glycol): pH and Fluorescence Measurements*, in press.
(5) Hemker, D. J.; Garza, V.; Frank, C. W. *Complexation of Poly(acrylic acid) and Poly(methacrylic acid) with Pyrene End-Labeled Poly(ethylene glycol): pH and Fluorescence Measurements*, in press.
(6) Tsuchida, E.; Osada, Y.; Ohno, H. *J. Macromol. Sci. Phys.* **1980**, *B17* (4), 683.
(7) Ohno, H.; Matsuda, H.; Tsuchida, E. *Makromol. Chem.* **1981**, *182*, 2267.
(8) Flamberg, A.; Pecora, R. *J. Phys. Chem.* **1984**, *88*, 3026.
(9) Tsuchida, E.; Abe, K. *Adv. Polym. Sci.* **1982**, 45.
(10) Bekturov, E.; Bimendina, L. A. *Adv. Poly. Sci.* **1981**, *41*, 99.
(11) Witten, T. A., Jr.; Sander, L. M. *Phys. Rev. Lett.* **1981**, *47*, 1400.
(12) Allcock, H. R.; Lampe, F. W. *Contemporary Polymer Chemistry*; Prentice-Hall: Englewood Cliffs, NJ, 1981.
(13) Meakin, P. *Phys. Rev. Lett.* **1983**, *51*, 1119.
(14) Kolb, H.; Botet, R.; Jullien, R. *Phys. Rev. Lett.* **1983**, *51*, 1123.
(15) Botet, R.; Jullien, R.; Kolb, M. *J. Phys. A: Math. Gen.* **1984**, *17*, 175.
(16) Schaefer, D. W.; Martin, J. E.; Wiltzius, P.; Cannell, D. S. *Phys. Rev. Lett.* **1984**, *52*, 2371.
(17) Weitz, D. A.; Huang, J. S.; Lin, M. Y.; Sung, J. *Phys. Rev. Lett.* **1985**, *54*, 1657.
(18) Hurd, A. J.; Schaefer, D. W. *Phys. Rev. Lett.* **1985**, *54*, 1043.
(19) Von Smoluchowski, M. *Phys. Z.* **1916**, *17*, 593.
(20) Sonntag, H.; Strenge, K. *Coagulation Kinetics and Structure Formation*; Plenum Press: New York, 1987; p 58.
(21) Pecora, R., Ed. *Dynamic Light Scattering: Applications of Photon Correlation Spectroscopy*; Plenum Press: New York, 1985.
(22) Bender, T. M.; Pecora, R. *J. Colloid Interface Sci.* **1988**, *126*, 638.
(23) Bender, T. M. Ph.D. Thesis, Stanford University, Stanford, CA, 1985.
(24) Aragon, S. R.; Pecora, R. *J. Chem. Phys.* **1976**, *64*, 2395.
(25) Billmeyer, F. W., Jr. *Textbook of Polymer Science*, 2nd ed., Wiley: New York, 1971; p 30.
(26) Thisted, R. A. *Elements of Statistical Computing: Numerical Computation*; Chapman and Hall: New York, 1987.
(27) Martin, J. E.; Schaefer, D. W. *Phys. Rev. Lett.* **1984**, *53*, 2457.
(28) Mandelbrot, B. B. *The Fractal Geometry of Nature*; Freeman: San Francisco, 1982.
(29) Weitz, D. A.; Lin, M. Y.; Huang, J. S. *Fractals and Scaling in Kinetic Colloid Aggregation*; Exxon Monograph; 1987.
(30) Provencher, S. W. *Makromol. Chem.* **1979**, *180*, 201.
(31) Provencher, S. W. *CONTIN User's Manual*; European Molecular Biology Laboratory Technical Report No. MBL-DA02; Heidelberg, 1980.
(32) Chen, S. H.; Chu, B.; Nossal, R., Eds. *Scattering Techniques Applied to Supramolecular and Nonequilibrium Systems*; Plenum Press: New York, 1981; p 87.
(33) Berne, B. J.; Pecora, R. *Dynamic Light Scattering*; Wiley-Interscience: New York, 1976.
(34) Pecora, R., Ed. *Dynamic Light Scattering: Applications of Photon Correlation Spectroscopy*; Plenum Press: New York, 1985.
(35) Flamberg, A.; Pecora, R. *J. Phys. Chem.* **1984**, *88*, 3026.
(36) Provencher, S. W. *Comput. Phys. Commun.* **1982**, *27*, 229.
(37) Provencher, S. W. *Comput. Phys. Commun.* **1982**, *27*, 213.
(38) Provencher, S. W. *Makromol. Chem.* **1979**, *180*, 201.
(39) Provencher, S. W.; Hendrix, J.; De Maeyer, L.; Paulussen, N. *J. Chem. Phys.* **1978**, *69*, 4273.